

Shape effect on the valley splitting in lead selenide nanowires

I. D. Avdeev*

Ioffe Institute, St. Petersburg 194021, Russia

We study the cross-section shape and size effects on the valley splitting in PbSe nanowires within the framework of empirical $sp^3d^3s^*$ tight-binding method. We consider idealized prismatic nanowires, grown along [110], with the cross-section shape varying from rectangular (terminated by {001} and {110} facets) to rhombic (terminated mostly by {111} facets). The valley splitting energies have the maximal value (up to hundreds meV) in rectangular nanowires, while in rhombic ones they are almost absent. The shape dependence is shown to be similar for a wide range cross-section sizes and different point symmetries of nanowires.

I. INTRODUCTION

Lead chalcogenide nanowires (NWs) have a wide range of possible applications. They can be used as circuit components [1, 2], light emitting (detecting) [3, 4] and energy harvesting [5, 6] devices. Throughout the past decades a big effort has been made towards experimental NW growth techniques [7–12]. They include colloidal synthesis [10], solution-liquid-solid [12] methods and even oriented attachment of lead salt nanocrystals [8]. Nowadays it is not only possible to grow a nanowire a few nm thin [13], but also to control its shape [14–16], size [17] and growth direction [18]. Nonetheless, theoretical modelling of lead chalcogenide NWs is quite challenging due to the multivalley band structure and strong intervalley coupling in these systems. It was shown [19] that the valley splitting can exceed the excitonic exchange splitting, so the study of the valley splitting is very important to understand the fundamental electronic and optical properties of PbSe NWs.

Lead selenide is a narrow direct band gap semiconductor (0.17 eV [20]) with the band extrema located at four inequivalent L valleys. In bulk crystal the ground electron and hole states are eight-fold degenerate by spin and valley degree of freedom, while in NWs this degeneracy is removed. There are two main mechanisms that split the valley multiplets (sets of confined states originated from different valleys) in PbSe NWs: the mass anisotropy [21] and the intervalley coupling [22] at the NW surface [23]. The first one is readily incorporated in the $\mathbf{k} \cdot \mathbf{p}$ and splits the valley multiplets in NWs only partially [21]. The second one fully removes the valley degeneracy and can be included in the $\mathbf{k} \cdot \mathbf{p}$ phenomenologically [23], but for careful theoretical description it requires an atomistic approach [24, 25] as it is very sensitive to the microscopic structure of the NW [26, 27].

It was shown [27] for cylindrical PbSe NWs and spherical quantum dots [26], that the valley splitting depends on diameter and the point symmetry of the considered structure. In this work we also take the shape of the NW into account. Following the theoretical [28, 29] and experimental [8] data, PbSe nanowires tend to have faceted

structure, therefore instead of cylindrical it is more convenient to consider prismatic shape of the NWs. For simplicity we consider idealized prismatic wires, carved out from ideal bulk PbSe crystal. With this approach, the microscopic structure of NWs is fully determined by the cross section and the spatial orientation of the covering prism. Even though the most natural growth direction of PbSe NWs is [001] [8], we consider [110] as the growth direction for the following reason: along this axis the two pairs of the L valleys remain inequivalent [25] which allows us to explicitly evaluate the valley splitting energies for each pair and study their dependencies on the NW shape parameters.

Among many atomistic methods we chose the empirical tight binding approach in nearest neighbour approximation, proved to be useful for many cubic semiconductors [30]. The use of the recent parametrization [26], which accurately reproduces experimental effective masses in the L valleys and show good agreement with experiment [31], allow us to study a wide range of NW sizes and shapes. We neglect the surface passivation, as the surface states in highly ionic crystals lie far outside the band gap [22] and there is no need to saturate the dangling bonds [25]. Note, even though the *ab initio* methods, such as DFT [32, 33] and GW [34, 35], are more accurate, complexity and demand in computational power make them hardly applicable to relatively large structures (more than a few hundreds of atoms).

In this paper we show, that the valley splitting drastically depends on the NW shape. The valley splitting is almost absent in NWs with the surface terminated mostly by {111} facets and has the maximal value in NWs with {110} and {001} terminated surface. We also notice that these are the most stable PbSe surfaces [28, 29]. Despite the polar nature, the {111} facets are also present in real systems, especially in colloidal solvents, where they can be passivated by ligands [33, 36].

II. VALLEY COUPLING IN NANOWIRES

The structure of the valley splittings is easier to analyse using the perturbative approach [23]. Without the valley coupling all the L valleys are independent and their energy spectra are fully determined by mass anisotropy [21]

* ivan-avdeev505@mail.ru

and quantum confinement [37]. The latter we associate with a set of quantum numbers q , well established for cylindrical PbSe nanowires [27]. It is important, that sets of states with a certain q (valley multiplets) are well distinguishable in the tight binding [27, 38, 39], where we consider the abrupt NW boundary as a perturbation that mix the valley states.

For further discussion, we enumerate the L valleys and corresponding wave vectors \mathbf{k} by index $\mu \in \{0, 1, 2, 3\}$

$$\begin{aligned} \mathbf{k}_0 &= \frac{\pi}{a} (1, 1, 1) & \mathbf{k}_1 &= \frac{\pi}{a} (-1, -1, 1), \\ \mathbf{k}_2 &= \frac{\pi}{a} (1, -1, -1) & \mathbf{k}_3 &= \frac{\pi}{a} (-1, 1, -1), \end{aligned} \quad (1)$$

where a is the lattice constant. In idealized NWs with translation period $\mathbf{T} = a(1, 1, 0)/2$ two of the valleys, L_0 and L_1 , project on the NW axis to the edge of the NW's Brillouin zone ($k = \pi/T$), while the others, L_2 and L_3 , to the Γ point ($k = 0$). Therefore $L_0 \rightarrow L_1$ and $L_2 \rightarrow L_3$ intervalley scattering processes are independent. In each of them, the mass anisotropy does not contribute to the valley splitting, since $m_0^* = m_1^*$ and $m_2^* = m_3^*$ with respect to the NW axis. Following [26] one may estimate the matrix element of the intervalley scattering at the NW surface as

$$M_{\mu,\nu} = C \sum_n e^{-i(\mathbf{k}_\mu - \mathbf{k}_\nu) \cdot \mathbf{R}_n} \Phi_\mu^*(\mathbf{R}_n) \Phi_\nu(\mathbf{R}_n), \quad (2)$$

where Φ is an envelope function, \mathbf{R}_n is a lattice node and C is a microscopic constant, an integral over the primitive cell. Despite the deceptive simplicity, evaluation of the matrix element is difficult as one has to compute the microscopic constant, exact envelopes and deal with the spin degeneracy. The spin can not be excluded due to its strong influence on the PbSe bandstructure. Eq. (2), however, helps to compare the two $L_0 \rightarrow L_1$ and $L_2 \rightarrow L_3$ scatterings processes. One can show, that the phase factors, $e^{-i(\mathbf{k}_0 - \mathbf{k}_1) \cdot \mathbf{R}_n}$ and $e^{-i(\mathbf{k}_2 - \mathbf{k}_3) \cdot \mathbf{R}_n}$, are the same, which assumes similar dependencies of the valley splitting on the microscopic NW structure.

For numerical simulations we use the supercell approach [40] without accounting for surface reconstruction and relaxation. We control the structure of NW supercells by four integers: size parameter $N > 0$, shape parameter M ($0 \leq M \leq N$), and two additional numbers $dN_1, dN_2 \in \{0, 1\}$ to adjust the NW symmetry. The NW supercells are prepared in two steps: first we make a parallelepiped consisting of $(2N + 2 + dN_1) \times (2N + 1 + dN_2)$ atomic layers along the $[\bar{1}10]$ and $[001]$ directions. Due to the periodicity, the supercell is only 2 atomic layers thick along the translation vector \mathbf{T} . Then we form the NW shape by cutting M $\{111\}$ atomic layers from the corners of the parallelepiped along $[1\bar{1}1]$ and $[\bar{1}11]$ directions, as shown in Fig. 1. Below we will refer the NWs with $M = 0$ as “rectangular” and the ones with $M = N$ as “rhombic”.

In total we consider four different NW types with D_{2h} (I), C_{2v} (II, III) and C_{2h} (IV) symmetries, summarized in Table I. Note that NWs of type II and III have different orientation of C_2 axes and the NWs of type IV have

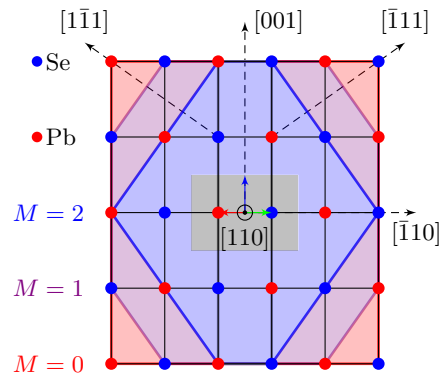


FIG. 1. $[110]$ view onto the NW supercells of type II with size parameter $N = 2$ and different shape parameters M . The supercells with $M = 0, 1, 2$ are enclosed in red (rectangular), violet and blue (rhombic) regions. The gray region in the middle corresponds to the smallest possible supercell of type II, shown also in Table I. The small RGB arrows show the xyz crystallographic axes.

non symmorphic spatial group. More details on the NW symmetry is given in Appendix A.

III. RESULTS AND DISCUSSION

In this work we focus on NWs of intermediate size, where the valley splittings are large enough and the NWs are not too small. It was shown [27], that the valley splitting is negligible (compared to exchange energy [19]) in relatively large systems and is the most pronounced for wires with diameters $\lesssim 50$ Å. Here we limit ourselves with size parameters $2 \leq N \leq 9$ corresponding to the range of NW cross section sizes from ≈ 10 to ≈ 50 Å.

Regarding the symmetry, the first three types of NWs are simple. Indeed, the only spinor representations of D_{2h} (type I) and C_{2v} (II, III) are two dimensional Γ_5^\pm and Γ_5 , respectively [41]. In the D_{2h} NWs, with inversion center being at cation, consecutive valley multiplets have opposite parity, therefore the valley multiplets are split via self-scattering at the NW surface. In the C_{2v} NWs, the lack of spatial inversion also allows for the valley coupling with high energy multiplets, though this assumed

TABLE I. Four considered NW types and their smallest supercells ($N = 0$). The cation, located at $(0, 0, 0)$ in the bulk coordinates frame, is marked with “x”.

NW Type	I	II	III	IV
symmetry	D_{2h}	C_{2v}	C_{2v}	C_{2h}
dN_1, dN_2	1, 0	0, 0	1, 1	0, 1

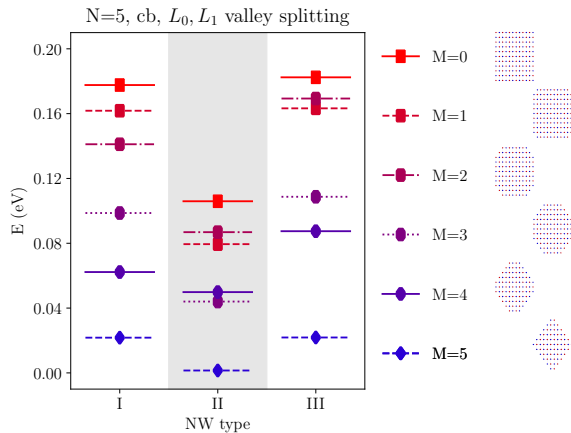


FIG. 2. Valley splitting energies of the L_0, L_1 ground conduction multiplet in NWs of type I, II and III as a function of shape parameter M . Corresponding NW supercells (of type II) are shown on the right. The size parameter $N = 5$.

to be negligible. In the C_{2h} NWs (type IV), the spatial symmetry forbids the splitting of the L_0, L_1 multiplets and the main mechanism of the L_2, L_3 valley splitting becomes the coupling with high energy states. Detailed analysis of this case is given below and in Appendix B.

In Fig. 2 we show the valley splitting energies of the L_0, L_1 ground conduction multiplet as a function of the shape parameter M in NWs of the first three types (see Table I) with the shape parameter $N = 5$ (approximate lateral size 25×30 Å). The valley splittings are maximal in rectangular NWs ($M = 0$) and almost absent in rhombic NWs ($M = N$). These NWs have their surfaces terminated either by $\{001\}$ and $\{110\}$ facets, or mostly by $\{111\}$ facets, respectively. The very similar dependence on the parameter M holds for each N . Even though the $\{111\}$ facets of PbSe are polar, in this work we assume that this charge is compensated and therefore neglect the built-in electric field. Note that the NWs of type III have one extra $(\bar{1}10)$ and one extra (001) atomic planes compared to the NWs of type II, but their splitting energies of the ground L_0, L_1 multiplet are almost twice as large. The type IV is not shown here, as in this case the L_0, L_1 valley multiplet acquires an extra degeneracy due to the time reversal symmetry, see Appendix B.

The valley splitting energies of the L_2, L_3 ground conduction multiplet as a function of the shape parameter M in NWs with $N = 5$ are summarized in Fig. 3. They are only about two thirds of the corresponding splittings of the L_0, L_1 multiplet, which is mostly due to the mass anisotropy. Indeed, the L_2 and L_3 valleys lie within (110) plane, while the L_0 and L_1 are tilted towards the wire axis and therefore have lighter effective in-plane masses, see (A2). Also note, that there is almost no difference in splitting energies in the NWs of type II and III.

Now let us turn to the NWs of type IV, shown in right column in Fig. 3. In these NWs the L_2 and L_3 ground

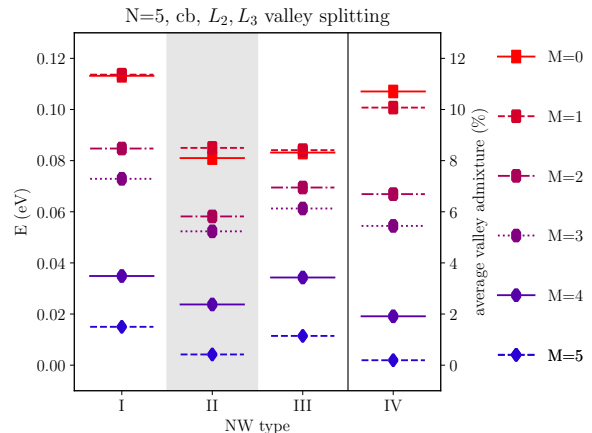


FIG. 3. NW types I, II, III: same as in Fig. 2, but for the L_2, L_3 ground conduction multiplet. NW type IV: relative average valley admixture, $(\Delta\rho_2 + \Delta\rho_3)/2$, as a function of shape parameter M . The size parameter $N = 5$.

valley multiplet is split via completely different mechanism. Since inversion center in NWs of type IV is located between atoms (see Table I), the L_2 and L_3 valleys have different parity and can not mix directly. The parity of an L_μ valley is related to phase factors $e^{i\mathbf{k}_\mu \cdot \mathbf{R}}$ at lattice nodes. For $\mathbf{R} = \pm a(0, 1, 1)/4$, positions of the two closest to inversion center cations, these phases are $\mp i$ for the L_2 valley and 1 for the L_3 . This implies that L_2 (L_3) valley is odd (even) and that the valley coupling in this case is only possible via far energy states.

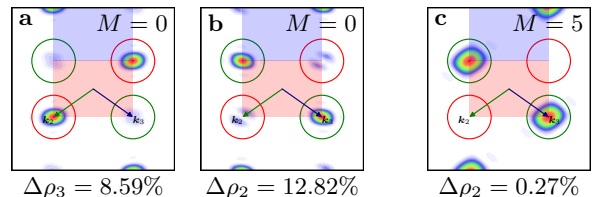


FIG. 4. kLDOS of the L_2, L_3 ground conduction multiplet states in NWs of the type IV. (a) Admixture of L_2 valley state to L_3 valley state in rectangular NW. (b) Admixture of L_3 to L_2 in rectangular NW, (c) same in rhombic NW. Red (green) circles show the area used to estimate the local density $\rho_{2(3)}$ near the $L_{2(3)}$ valley. The size parameter $N = 5$.

In fact, this possibility is realized and is the most pronounced in rectangular NWs (shape parameter $M = 0$), similarly to the valley splittings. To illustrate this, in Fig. 4 we show the local density of states in reciprocal space (kLDOS, see Refs. [27, 42] for details). For quantitative description of the valley coupling we introduce “valley admixture”

$$\Delta\rho_{2(3)} = \frac{\rho_{2(3)}}{\rho_2 + \rho_3}, \quad (3)$$

where $\rho_{2(3)}$ is the valley density, integrated over small re-

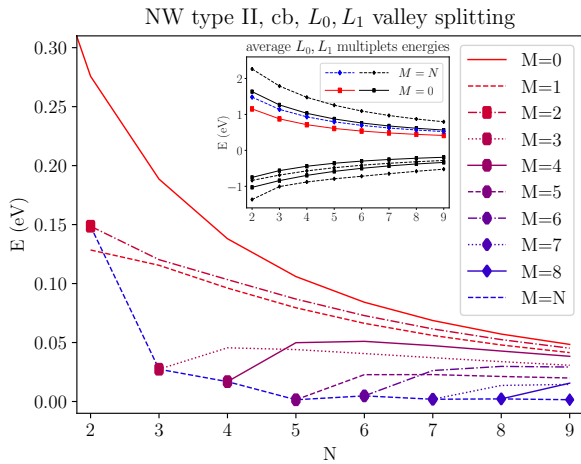


FIG. 5. The valley splitting energies of the L_0, L_1 ground conduction multiplet in NWs of type II as a function of the NW shape (M) and size (N) parameters. Lines connect data point with the same M . Each line starts from $N = M$ (indicated by marker) and has a unique combination of color and style. Inset: average energies of the two lowest energy valley multiplets in conduction and valence bands in rhombic ($M = N$, solid) and rectangular ($M = 0$, dashed) NWs as a function of their size parameter N .

gion near the L_2 (L_3) valley shown by red (green) circles in Fig. 4. One can see that the valley admixture in rectangular NWs is much higher than in rhombic ones. The value $\Delta\rho_3$ in rhombic NW ($M = N = 5$) is 0.11% and the corresponding kLDOS is not shown in Fig. 4. The density distributions near the main peaks in Figs. 4a–4c are s -like (correspond to the ground multiplet), while distributions near the secondary peaks in Figs. 4a and 4b are d - and p -like, respectively. It proves that the admixed states belong to different valley multiplets. Note, for convenience in Fig. 3 we show the average valley admixtures $(\Delta\rho_2 + \Delta\rho_3)/2$ for the NWs of type IV.

Before we discussed NWs with the size parameter $N = 5$ (ten atomic layers along the $[001]$ and $[\bar{1}10]$ directions). Next, in Figs. 5 and 6 we show both size (N) and shape (M) dependencies of the valley splitting. We show the data only for the NWs of type II, since the others behave very similar. We vary the size parameter N from 2 to 9 so the lateral size of NWs changes from $11 \times 12 \text{ \AA}^2$ to $41 \times 55 \text{ \AA}^2$ along the $[\bar{1}10]$ and $[001]$ axes respectively. In order to highlight the shape and size dependencies, in Figs. 5 and 6 we connect data points with the same parameter M by color lines (solid red for $M = 0$, dashed blue for $M = N$). For each size parameter N , the shape parameter M satisfies $0 \leq M \leq N$, therefore each line in Figs. 5 and 6 starts from $N = M$. The starting point of each line (except for $M = 0$ and $M = N$) is indicated by marker.

Fig. 5 shows the valley splitting energies of the L_0, L_1 ground conduction multiplet. Inset shows the average

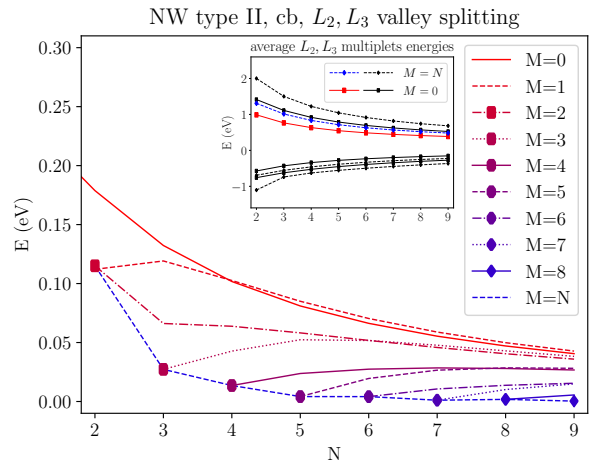


FIG. 6. Same as in Fig. 5, but for L_2, L_3 multiplets.

energies (without the valley splitting) of the two valley multiplets with lowest energies in conduction and valence bands in rectangular ($M = 0$, dashed lines) and rhombic ($M = N$, solid lines) NWs as a function of size parameter N . Average energies of the ground conduction multiplet are additionally indicated by color to match the main plot (red for $M = 0$, blue for $M = N$). Note, that the rhombic NWs exhibit larger confinement energies than their rectangular counterparts, while the valley mixing in rhombic NWs is strongly suppressed.

The same data for the L_2, L_3 ground conduction multiplet is shown in Fig. 6. We do not discuss it in details, but mention, that all the size and shape dependencies of the valley splitting (coupling) are almost the same, except for their absolute values. Therefore we conclude, that the shape induced suppression of the valley splitting in NWs is rather a physical phenomena.

IV. CONCLUSION

We studied the valley splitting in $[110]$ -grown nanowires with different size, shape and symmetry. We demonstrate, that the valley splittings substantially depend on the NW shape, for particular case of prismatic octagonal NWs which is determined by relative fraction of $\{001\}, \{110\}$ facets compared to $\{111\}$ facets at the NW surface. The values of valley splittings are large, up to 100 meV in NWs about 5 nm diameter. The splittings tend to have maximal values in rectangular NWs ($\{001\}$ and $\{110\}$ facets at the surface) and are almost absent in rhombic NWs (mostly $\{111\}$ facets at the surface). This result holds for a wide range of NW sizes and different point symmetries.

We also found a special type of NWs with non symmorphic spatial group, where L_0, L_1 valley multiplets become fourfold degenerate and the splitting of L_2, L_3 multiplets is due to the intervalley coupling via far energy states

Results of this work, except for the absolute values of the valley splittings, also apply for PbS and PbTe, due to the very similar band structures of these materials.

ACKNOWLEDGMENTS

The author acknowledges fruitful discussions with M. O. Nestoklon and financial support by RFBR Project No. 17-02-00383 A.

Appendix A: Microscopic wire structure

PbSe has the rocksalt crystal structure with

$$\mathbf{a}_1 = \frac{a}{2}(1, 0, 1), \quad \mathbf{a}_2 = \frac{a}{2}(1, 1, 0), \quad \mathbf{a}_3 = \frac{a}{2}(0, 1, 1) \quad (\text{A1})$$

lattice vectors, where $a = 6.1 \text{ \AA}$ is the lattice constant [26]. Reciprocal lattice vectors are conveniently related with the L valleys $\mathbf{1}$ as $\mathbf{b}_\mu = 2\mathbf{k}_\mu, \mu = 1, 2, 3$.

With the used tight binding parametrization [26] the first conduction band effective mass ratios along the $[\bar{1}10]$, $[001]$ and $[110]$ directions (xyz NW axes) are

$$\frac{m_{0(1)}^{[\bar{1}10]}}{m_{2(3)}^{[\bar{1}10]}} = 0.74, \quad \frac{m_{0(1)}^{[001]}}{m_{2(3)}^{[001]}} = 1, \quad \frac{m_{0(1)}^{[110]}}{m_{2(3)}^{[110]}} = 1.36, \quad (\text{A2})$$

where $m_{\mu(\nu)}^{\mathbf{n}}$ denotes the effective mass along \mathbf{n} of the first conduction band electron at the $L_{\mu(\nu)}$ valley.

The first three NW types, see Table I, have D_{2h} , C_{2v} and C_{2v} point groups, respectively. Their symmetries are determined by orientation of C_2 axes and the position of the point symmetry origin relative to the $(0, 0, 0)$ cation, marked by “x” in Table I. NW type I has inversion center, three C_2^x, C_2^y, C_2^z rotation axes (in the NW coordinates frame) and three corresponding reflection planes $\sigma_v^x, \sigma_v^y, \sigma_v^z$. NW type II has C_2^x rotation axis and σ_v^y, σ_v^z reflection planes with the point symmetry origin being at $a(-1, 1, 0)/8$. NW type III has C_2^y rotation axis and σ_v^x, σ_v^z reflection planes with the point symmetry origin being at $a(0, 0, 1)/4$.

NW type IV has non symmorphic spatial group with C_{2h} point symmetry. We use $a(-1, 1, 2)/8$ point (relative to the $(0, 0, 0)$ cation) as the point symmetry origin, which results in the following quotient group

$$\left\{ e, a = \left(C_2^z, \frac{\mathbf{a}_3}{2} \right), b = (\sigma_h^z, \mathbf{0}), ab = \left(i, \frac{\mathbf{a}_3}{2} \right) \right\}. \quad (\text{A3})$$

Note, that this is not the only possible, but is the most convenient way to choose the point symmetry origin.

Appendix B: Symmetry analysis

Symmetry analysis for the first three NW types is trivial and therefore omitted. Instead, we focus on the NW

type IV to describe the absence of the valley splitting in L_0, L_1 valley multiplets.

Following ref. [43], we use projective representations to classify the states of L_0, L_1 valley multiplets, because these valleys project onto the edge of the NW Brillouin zone. In C_{2h} there are two projective classes: K_0 and K_1 . Class K_0 has only one dimensional (vector and spinor) representations [41], while in K_1 there is only one two-dimensional representation $P^{(1)}$.

Since the L_2, L_3 valleys project onto the Γ point, states of the L_2, L_3 multiplets belong to the class K_0 and can be classified according to ref. [41]. States of the L_0, L_1 valley multiplets belong to the class K_1 , and therefore transform according to $P^{(1)}$. Indeed, the factor system

$$\omega_{\mathbf{k}}(g_1, g_2) = e^{i(\mathbf{k} - R_1^{-1}\mathbf{k})\boldsymbol{\tau}_2} \quad (\text{B1})$$

on elements (A3) with $\mathbf{k} = \mathbf{k}_0$ or $\mathbf{k}_1, (1)$, has the form

$$\omega_{\mathbf{k}_{0(1)}}(a^k b^p, a^{k'} b^{p'}) = \alpha^{(pk')} \quad \alpha = -1, \quad (\text{B2})$$

which is the standard form for the class K_1 [43]. Note, since all $\boldsymbol{\tau} \parallel [110]$, the factor system depends only on projection of the wave vector \mathbf{k} onto the NW axis.

Next we consider time reversal symmetry by means of Herring criterion [43, 44], which is about relation of ψ and $\hat{T}\psi$, where \hat{T} is the time reversal operator. The criterion reads as a sum over quotient group

$$\frac{1}{h} \sum_{g \in G/T} \chi(g^2) = \begin{cases} K^2, & (a) \\ 0, & (b) \\ -K^2, & (c) \end{cases}, \quad \hat{T}^2 = K^2 \hat{T}. \quad (\text{B3})$$

There are three options: ψ and $\hat{T}\psi$ are (a) linearly dependent, (b) linearly independent and transform according to conjugate representations or (c) equivalent representations. In cases (b) and (c) time reversal symmetry leads to additional degeneracy of states.

The fact that the factor system for L_0, L_1 multiplets, eq. (B2), has the standard form, allow us to use the explicit form of generator matrices $a = \sigma_z, b = \sigma_x$ for $P^{(1)}$ representation from ref. [43]. With generators matrices the sum (B3) for L_0, L_1 states is easily evaluated

$$\frac{2 + \text{Tr}(\sigma_z^2) + \text{Tr}(\sigma_x^2) - \text{Tr}(\sigma_y^2)}{4} = 1 = -K^2 \quad (\text{B4})$$

and we see that the case (c) is realized. Here $K^2 = -1$ due to the antiunitary nature of time reversal operator \hat{T} for spinors. Therefore the states of L_0, L_1 multiplets are fourfold degenerate.

Note, that for L_2, L_3 states, the case (b) is realized, so all the states of L_2, L_3 multiplets are twice degenerate. We also note, that evaluation of the sum (B3) in this case is much simpler using the double group approach [41], instead of projective representations theory.

- [1] Dmitri V. Talapin and Christopher B. Murray, "Pbse nanocrystal solids for n- and p-channel thin film field-effect transistors," *Science* **310**, 86–89 (2005).
- [2] David K. Kim, Tarun R. Vemulka, Soong Ju Oh, Weon-Kyu Koh, Christopher B. Murray, and Cherie R. Kagan, "Ambipolar and unipolar pbse nanowire field-effect transistors," *ACS Nano*, *ACS Nano* **5**, 3230–3236 (2011).
- [3] Vlad Sukhovatkin, Sean Hinds, Lukasz Brzozowski, and Edward H. Sargent, "Colloidal quantum-dot photodetectors exploiting multiexciton generation," *Science* **324**, 1542–1544 (2009).
- [4] Lazaro A. Padilha, Gero Nootz, Scott Webster, David J. Hagan, Eric W. Van Stryland, Larissa Levina, Vlad Sukhovatkin, and Edward H. Sargent, "Two-photon absorption and multi-exciton generation in lead salt quantum dots," in *Ultrafast Phenomena in Semiconductors and Nanostructure Materials XIV*, edited by Jin-Joo Song, Kong-Thon Tsen, Markus Betz, and Abdulkhakem Y. Elezzabi (SPIE-Intl Soc Optical Eng, 2010).
- [5] Felice Gesuele, Chee Wei Wong, Matt Sfeir, Weon kyu Koh, Chris B. Murray, and Tony Heinz, "Ultrafast supercontinuum spectroscopy of multiple exciton states in lead chalcogenide nanorods and nanocrystals," in *Conference on Lasers and Electro-Optics 2012* (Optical Society of America, 2012) p. QM2G.2.
- [6] Nathaniel J. L. K. Davis, Marcus L. Böhm, Maxim Tabachnyk, Florencia Wisnivesky-Rocca-Rivarola, Tom C. Jellicoe, Caterina Ducati, Bruno Ehrler, and Neil C. Greenham, "Multiple-exciton generation in lead selenide nanorod solar cells with external quantum efficiencies exceeding 120%," *Nature Communications* **6**, 8259 (2015).
- [7] E. Lifshitz, M. Bashouti, V. Kloper, A. Kigel, M. S. Eisen, and S. Berger, "Synthesis and characterization of PbSe quantum wires, multipods, quantum rods, and cubes," *Nano Letters* **3**, 857–862 (2003).
- [8] Kyung-Sang Cho, Dmitri V. Talapin, Wolfgang Gaschler, and Christopher B. Murray, "Designing pbse nanowires and nanorings through oriented attachment of nanoparticles," *Journal of the American Chemical Society*, *Journal of the American Chemical Society* **127**, 7140–7147 (2005).
- [9] M. Fardy, A.I. Hochbaum, J. Goldberger, M.M. Zhang, and P. Yang, "Synthesis and thermoelectrical characterization of lead chalcogenide nanowires," *Advanced Materials* **19**, 3047–3051 (2007).
- [10] Dmitri V. Talapin, Heng Yu, Elena V. Shevchenko, Arun Lobo, and Christopher B. Murray, "Synthesis of colloidal pbse/pbs core-shell nanowires and pbs/au nanowire nanocrystal heterostructures," *The Journal of Physical Chemistry C*, *The Journal of Physical Chemistry C* **111**, 14049–14054 (2007).
- [11] Weon-kyu Koh, Adam C. Bartnik, Frank W. Wise, and Christopher B. Murray, "Synthesis of monodisperse PbSe nanorods: A case for oriented attachment," *J. Am. Chem. Soc.* **132**, 3909–3913 (2010).
- [12] Javeed Akhtar, Masood Akhtar, Mohammad Azad Malik, Paul O'Brien, and James Raftery, "A single-source precursor route to unusual pbse nanostructures by a solution-liquid-solid method," *Journal of the American Chemical Society*, *Journal of the American Chemical Society* **134**, 2485–2487 (2012).
- [13] Rion Graham and Dong Yu, "High carrier mobility in single ultrathin colloidal lead selenide nanowire field effect transistors," *Nano Letters*, *Nano Letters* **12**, 4360–4365 (2012).
- [14] Young-wook Jun, Jin-sil Choi, and Jinwoo Cheon, "Shape control of semiconductor and metal oxide nanocrystals through nonhydrolytic colloidal routes," *Angewandte Chemie International Edition* **45**, 3414–3439 (2006).
- [15] Taleb Mokari, Minjuan Zhang, and Peidong Yang, "Shape, size, and assembly control of pbte nanocrystals," *Journal of the American Chemical Society*, *Journal of the American Chemical Society* **129**, 9864–9865 (2007).
- [16] Ali M. Jawaid, Daniel J. Asunskis, and Preston T. Snee, "Shape-controlled colloidal synthesis of rock-salt lead selenide nanocrystals," *ACS Nano* **5**, 6465–6471 (2011).
- [17] Diogenes Placencia, Janice E. Boercker, Edward E. Foos, and Joseph G. Tischler, "Synthesis and optical properties of PbSe nanorods with controlled diameter and length," *J. Phys. Chem. Lett.* **6**, 3360–3364 (2015).
- [18] So Young Jang, Yun Mi Song, Han Sung Kim, Yong Jae Cho, Young Suk Seo, Gyeong Bok Jung, Chi-Woo Lee, Jeunghee Park, Minkyung Jung, Jinhee Kim, Bongsoo Kim, Jin-Gyu Kim, and Youn-Joong Kim, "Three synthetic routes to single-crystalline pbs nanowires with controlled growth direction and their electrical transport properties," *ACS Nano*, *ACS Nano* **4**, 2391–2401 (2010).
- [19] J. M. An, A. Franceschetti, and A. Zunger, "The excitonic exchange splitting and radiative lifetime in pbse quantum dots," *Nano Letters* **7**, 2129–2135 (2007).
- [20] Su-Huai Wei and Alex Zunger, "Electronic and structural anomalies in lead chalcogenides," *Phys. Rev. B* **55**, 13605–13610 (1997).
- [21] A. C. Bartnik, Al. L. Efros, W.-K. Koh, C. B. Murray, and F. W. Wise, "Electronic states and optical properties of PbSe nanorods and nanowires," *Phys. Rev. B* **82**, 195313 (2010).
- [22] G. Allan and C. Delerue, "Confinement effects in PbSe quantum wells and nanocrystals," *Phys. Rev. B* **70**, 245321 (2004).
- [23] M. O. Nestoklon, L. E. Golub, and E. L. Ivchenko, "Spin and valley-orbit splittings in SiGe/Si heterostructures," *Phys. Rev. B* **73**, 235334 (2006).
- [24] J. M. An, A. Franceschetti, S. V. Dudiy, and Alex Zunger, "The peculiar electronic structure of pbse quantum dots," *Nano Letters*, *Nano Letters* **6**, 2728–2735 (2006).
- [25] Abhijeet Paul and Gerhard Klimeck, "Atomistic study of electronic structure of PbSe nanowires," *Applied Physics Letters* **98**, 212105 (2011).
- [26] A. N. Poddubny, M. O. Nestoklon, and S. V. Goupalov, "Anomalous suppression of valley splittings in lead salt nanocrystals without inversion center," *Phys. Rev. B* **86**, 035324 (2012).
- [27] I. D. Avdeev, A. N. Poddubny, S. V. Goupalov, and M. O. Nestoklon, "Valley and spin splittings in pbse nanowires," *Phys. Rev. B* **96**, 085310 (2017).
- [28] Mario Argeri, Alberto Fraccarollo, Fabio Grassi, Leonardo Marchese, and Maurizio Cossi, "Density functional theory modeling of pbse nanoclusters: Effect of

- surface passivation on shape and composition,” *The Journal of Physical Chemistry C*, **The Journal of Physical Chemistry C** **115**, 11382–11389 (2011).
- [29] Volker L. Deringer and Richard Dronskowski, “Stabilities and reconstructions of clean pbs and pbse surfaces: Dft results and the role of dispersion forces,” *The Journal of Physical Chemistry C* **120**, 8813–8820 (2016).
- [30] Jean-Marc Jancu, Reinhard Scholz, Fabio Beltram, and Franco Bassani, “Empirical *spds** tight-binding calculation for cubic semiconductors: General method and material parameters,” *Phys. Rev. B* **57**, 6493–6507 (1998).
- [31] Alexander N. Poddubny, Valentina M. Litvyak, Mikhail O. Nestoklon, Roman V. Cherbunin, Valerii V. Golubkov, Petr A. Onushchenko, Anastasiya N. Babkina, Alexei A. Onushchenko, and Serguei V. Goupalov, “Role of valley anisotropy in optical absorption of monodisperse pbs nanocrystals,” *The Journal of Physical Chemistry C*, **The Journal of Physical Chemistry C** **121**, 27766–27773 (2017).
- [32] E. O. Wrasse, R. J. Baierle, T. M. Schmidt, and A. Fazzio, “Quantum confinement and spin-orbit interactions in pbse and pbte nanowires: First-principles calculation,” *Phys. Rev. B* **84**, 245324 (2011).
- [33] Yun Liu, Donghun Kim, Owen P. Morris, David Zhitomirsky, and Jeffrey C. Grossman, “Origins of the stokes shift in pbs quantum dots: Impact of polydispersity, ligands, and defects,” *ACS Nano*, **ACS Nano** **12**, 2838–2845 (2018).
- [34] Kerstin Hummer, Andreas Grüneis, and Georg Kresse, “Structural and electronic properties of lead chalcogenides from first principles,” *Phys. Rev. B* **75**, 195211 (2007).
- [35] A. Svane, N. E. Christensen, M. Cardona, A. N. Chantis, M. van Schilfgaarde, and T. Kotani, “Quasiparticle self-consistent *GW* calculations for PbS, PbSe, and PbTe: Band structure and pressure coefficients,” *Phys. Rev. B* **81**, 245120 (2010).
- [36] Danylo Zhrebetskyy, Marcus Scheele, Yingjie Zhang, Noah Bronstein, Christopher Thompson, David Britt, Miquel Salmeron, Paul Alivisatos, and Lin-Wang Wang, “Hydroxylation of the surface of pbs nanocrystals passivated with oleic acid,” *Science* (2014), 10.1126/science.1252727.
- [37] S. V. Goupalov, “Comment on “electronic structure and optical properties of quantum-confined lead salt nanowires”,” *Phys. Rev. B* **84**, 037303 (2011).
- [38] I D Avdeev and M O Nestoklon, “Electronic structure of PbSe nanowires,” *Journal of Physics: Conference Series* **769**, 012074 (2016).
- [39] J. Pawłowski, D. Żebrowski, and S. Bednarek, “Valley qubit in a gated **mos₂** monolayer quantum dot,” *Phys. Rev. B* **97**, 155412 (2018).
- [40] Peter YU and Manuel Cardona, *Fundamentals of Semiconductors: Physics and Materials Properties*, 4th ed. (Springer-Verlag Berlin Heidelberg, 2010).
- [41] George F. Koster, John O. Dimmock, Robert G. Wheeler, and Hermann Statz, *The Properties of the Thirty-Two Point Groups* (M.I.T. Press, Cambridge, 1963).
- [42] M. O. Nestoklon, A. N. Poddubny, P. Voisin, and K. Dohnalova, “Tuning optical properties of ge nanocrystals by si shell,” *The Journal of Physical Chemistry C* **120**, 18901–18908 (2016).
- [43] G.L. Bir and G.E. Pikus, *Symmetry and Strain-Induced Effects in Semiconductors* (Wiley, New York, 1974).
- [44] Conyers Herring, “Effect of time-reversal symmetry on energy bands of crystals,” *Phys. Rev.* **52**, 361–365 (1937).